ELSEVIER

Journal of Power Sources 110 (2002) 285–294

JOURNAL OF POWER SOURCES

www.elsevier.com/locate/jpowsour

Virtual test bed for advanced power sources

R.A. Dougal*, S. Liu, L. Gao, M. Blackwelder

Department of Electrical Engineering, University of South Carolina, Columbia, SC 29208, USA

Abstract

Design or analysis of advanced power systems, involves knowledge in many disciplines. This paper introduces the virtual test bed (VTB) computational environment for modeling, dynamic simulation and virtual-prototyping of such interdisciplinary systems. A basic feature of the VTB is that it allows experts to build models within their domain of expertise using tools with which they are familiar, then to execute those models in a system context. We describe here several studies which illustrate how VTB can be used in the study of systems containing electrochemical power sources. The multiple approaches to construct models and the capabilities to co-simulate with other software packages are also described.

Keywords: Battery; Interdisciplinary modeling; Resistive-companion method; Virtual test bed simulation

1. Introduction

The virtual test bed (VTB) [1] provides a unique capability for virtual-prototyping of advanced power systems. It can be of great value to the power source community by encapsulating knowledge of power source performance in the form of models that can be easily connected to other elements to allow study of power source performance in a system context (or conversely, study of the system performance in light of specific power source characteristics). It opens the possibility for others to gainfully apply the knowledge that has been so encapsulated.

The VTB can provide to the battery community a ''common language'' for expressing problems, a unique capability to help solve those problems, and a powerful means to explain the solutions. The software provides a path to a fully inclusive teaming environment, both because it allows team members to continue to use individual tools with which they are familiar (e.g. Matlab/Simulink®, Advanced Continuous Simulation Language (Avant!), etc.), and because it is freely available to every constituency.

In this paper, we will describe some of the features of the VTB and document some applications of the VTB to study of problems interesting to the power source community. Also, we will describe several of the battery models available for use in the VTB.

2. VTB features

The VTB (distributed freely by the University of South Carolina from http://vtb.engr.sc.edu/) provides capabilities to import dynamic models from a variety of environments (while enforcing data, signal, or natural coupling laws at the ''terminals''), to connect finite element models with lumped-element dynamic models, to import structural models that describe the physical properties of the system, and to create and drive advanced visualizations from within the simulation environment. There is a significant emphasis on re-use of existing computer data—both in dynamic models and in visualization models. Additional advanced capabilities have been demonstrated but are not yet available in the public version of the software. These advanced capabilities include distributed simulations over internet connections, and simulations with machinery in the loop. Refinements and generalizations of these capabilities are in progress and will later be available in the public version of the software. The VTB offers the following capabilities.

- A commonly available (Win NT) user environment.
- Advanced interactive visualization environment.
  - Visualization models can be easily created and linked to live simulation data. Visualization aids the user to rapidly comprehend the system performance. Visual outputs include data-driven animation of the motion of solid objects, imposition on top of the solid objects of novel representations of abstract simulation data, or simply oscilloscope-like graphs.

* Corresponding author. Tel.: +1-803-777-7890; fax: +1-803-777-8045.
E-mail address: dougal@engr.sc.edu (R.A. Dougal).

0378-7753/02/$ – see front matter © 2002 Published by Elsevier Science B.V.
PII: S0378-7753(02)00191-X

- Runtime user interaction with the simulation environment, including re-definition of individual components or system topology.
  - Users can change the system topology or parameters while a simulation executes. This allows the user to rapidly investigate interactions between components or to explore the influence of design parameters on system performance.
- A capability to reuse existing models, especially to import models from other environments.
  - Different languages can be used to build models of the different components that make up a system. This allows an individual to build models using the language preferred within his or her discipline.
- Web-based model library that is frequently updated.

Native models that must obey natural coupling laws (conservation of some quantity—charge, energy, mass, etc.) are coded in ''resistive-companion (RC) form'' which is essentially a discretized form of the differential–algebraic equations that represent the system, with explicit expression of the Jacobian. Formulating models in this way speeds the simulation and allows automatic enforcement of conservation laws at connections to other devices.

In addition, VTB provides tools for importing models from other environments, both from source code or as executables, and wrapping them so as to automate the enforcement of applicable conservation laws. Methods of completing the connection include latency methods, numerical or symbolic computation of the Jacobian, dependent sources, etc.

Applications of power sources such as batteries, fuel cells and solar arrays usually require interdisciplinary knowledge. The battery model described here was constructed in a close collaboration between the departments of electrical engineering and chemical engineering at the University of South Carolina. But once that knowledge was captured, the models can be productively used by others. We will describe here the process of building a native VTB model, then describe several applications that use that model (or similar models) in systems.

3. Modeling of electrochemical power sources

Native VTB models are coded in RC format [2], which allows definition of ''across'' and ''through'' variables which are subject to natural conservation laws [3]. This approach considers the fully-coupled equations for all processes, yielding the history of each process, the interactions between different processes, and the effect of each parameter on the dynamic system response.

The method of modeling a battery system in RC format will be explained by reference to a nickel hydrogen battery, for which the icon is shown in Fig. 1. Although the icon does not necessarily represent the actual physical configuration of the battery, it is sufficiently detailed to remind the user what it represents. The battery cells are shown housed in a

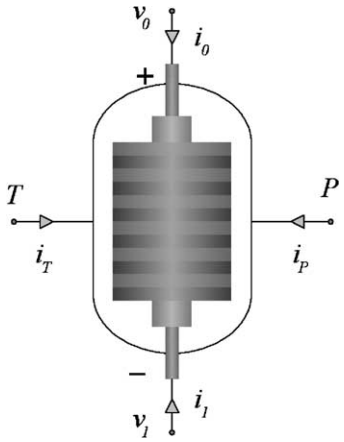

Fig. 1. Nickel hydrogen battery icon, labeled with definitions of quantities associated with the four terminals—two electrical, one thermal, and one pressure sensor.

cylindrical pressure vessel from which four terminals extend. The electrical terminals at the anode (v_0) and the cathode (v_1) transport electric power to the external circuit. The across and through variables for these nodes are the potential and the current, respectively. The thermal terminal (T) actually represents the entire external surface of the battery through which the heat is exchanged between the battery and the environment. The across variable for the thermal terminal is the bulk temperature of the battery, and the thermal current [4] is defined so that the heat power transferred at the terminal equals the product of the temperature and the thermal current. The pressure terminal (P) conveys the data from an implicit pressure sensor via a finite, but small output impedance (while future versions of the VTB computational system will comply with IEEE VHDL-AMS standards [3] with respect to object coupling methods: natural coupling, signal coupling and data coupling, the current release version of VTB treats all ports as natural ports). The pressure terminal is generally used to provide feedback to a controller.

The terminal voltage v_b of the battery is given as

$$V_b(t) = E_{eq}[T(t), x(t)] + i_b R_b[T(t)] \quad (1)$$

where T is the battery bulk temperature, x the state-of-discharge, and both are functions of the independent variable time t. For a simple model, the spatial variation of the temperature is ignored. At any instant, the battery current i_b, is determined by the rate of change of the state-of-discharge, as shown by Eq. (2):

$$i_b(t) = -Q_{max} \frac{dx}{dt} \quad (2)$$

where Q_{max} is the maximum charge stored in the active material. The battery voltage v_b and the current i_b can be related to the terminal variables by

$$v_b(t) = v_0(t) - v_1(t) \quad (3)$$

$$i_b(t) = i_0(t) = -i_1(t) \quad (4)$$

The resistance R_b of the battery appearing in Eq. (1) is due to the finite conductivity of separator and electrodes, and it is assumed to be rate-independent. In addition, kinetic resistance is ignored since it is generally small compared to ohmic resistance. The equilibrium potential E_{eq} is a direct result of electrochemical processes on the electrode. Depending upon the type of electrodes and the conditions under which chemical reactions take place, the potential usually is a strongly non-linear function of the temperature and the state-of-discharge. For a nickel hydrogen battery, the equilibrium potential is primarily determined by nickel reduction/oxidation at the positive electrode. Here, we assume that the kinetics of the chemical reactions are not limiting factors so that all intermediate reactions, side reactions, and hydrogen reaction at the negative electrode, as included in a full-scale model [5,6], can be ignored. The reaction at the nickel electrode is given by

$$\mathrm{Ni(OH)_2 + OH^- \Leftrightarrow NiOOH + H_2O + e^-} \tag{5}$$

and the associated equilibrium potential is given by

$$E_{eq}(T,x) = E^0_{eq}(T) + \frac{RT}{F}\ln\left(\frac{1-x}{x}\right) - \frac{RT}{2F}\left[A_0T(2-3.5x) + B_0T(2-6x+3x^2)\right] \tag{6}$$

where R and F are the gas constant and Faraday constant, respectively. For a given temperature, E^0_{eq} can be expressed as

$$E^0_{Ni}(T) = \begin{cases} 1.589 - 0.00084T, & \text{for } v_b < E_{eq} \\ 1.649 - 0.00084T, & \text{for } v_b \geq E_{eq} \end{cases} \tag{7}$$

where the differences between E^0_{eq} for charge and discharge account for cycling hysteresis [7,8] of nickel hydroxide, which is approximated by a constant 0.06 V. A_0 and B_0 in Eq. (6) are the so-called two-parameter activity coefficients [9] of the thermodynamics for nickel hydroxide reaction. They are given as

$$A_0(T) = -0.0231T + 11.5 \tag{8}$$

$$B_0(T) = 0.0492T - 19.4 \tag{9}$$

As can be seen from Eqs. (1) to (9), the current not only is a function of the battery voltage, but also of the temperature. An explicit relation between the current and voltage is impossible to find. However, it is unnecessary to do so since the method of VTB modeling is to convert the above mathematical descriptions into RC form by discretizing equations within one time step, so that the terminal through variables can be explicitly expressed as functions of the terminal across variables:

$$\begin{pmatrix} i_0(t) \\ i_1(t) \end{pmatrix} = \begin{pmatrix} g_{00} & g_{01} & g_{0T} & 0 \\ g_{10} & g_{11} & g_{1T} & 0 \end{pmatrix} \begin{pmatrix} v_0(t) \\ v_1(t) \\ T(t) \\ P(t) \end{pmatrix} - \begin{pmatrix} b_0(t-h) \\ b_1(t-h) \end{pmatrix} \tag{10}$$

where h is the time step. The conductance elements in Eq. (10) can be found as

$$g_{mn} = \left(\frac{\partial i_m}{\partial v_n}\right)_{t-h}, \quad \text{for } m = 0,1 \quad \text{and} \quad n = 0,1,T \tag{11}$$

and

$$b_0(t-h) = -b_1(t-h) = -i_0(t-h) + g_{00}v_0(t-h) + g_{01}v_1(t-h) + g_{0T}T(t-h) \tag{12}$$

Thermal processes in the battery are governed by the energy balance equation [10]. We ignore the heat due to change of specific heat, phase change, and mixing. The equation now becomes:

$$mc_p\frac{dT}{dt} = i_b v_b - i_b E_{eq} - i_b T\frac{dE_{eq}}{dT} + i_T T \tag{13}$$

where m is the battery mass, and c_p is the specific heat. The first and the fourth terms on the right-hand side represent to the electric work and heat exchanged with the surroundings, respectively. The second term is the portion of input power that is converted and stored in the battery as chemical energy, and the third term is the reversible heat power due to entropy change. Based on Eq. (13), the RC form for the thermal terminal can be written as

$$i_T(t) = \begin{pmatrix} g_{T0} & g_{T1} & g_{TT} & 0 \end{pmatrix} \begin{pmatrix} v_0(t) \\ v_1(t) \\ T(t) \\ P(t) \end{pmatrix} - (b_T(t-h)) \tag{14}$$

$$g_{Tn} = \left(\frac{\partial T}{\partial v_n}\right)_{t-h}, \quad n = 0,1,T \tag{15}$$

$$b_T(t-h) = -i_T(t-h) + g_{T0}v_0(t-h) + g_{T1}v_1(t-h) + g_{TT}T(t-h) \tag{16}$$

In viewing Eqs. (10)–(12) and (14)–(16), it is noticed that RC model equations for each terminal are of the same format. In fact, these equations can be applied to essentially any battery system or other interdisciplinary system. What makes the model specific is the governing equations and the definition of terminal variables. In addition, the method to seek the values of the conductance elements expressed by Eqs. (11) and (15) is the decisive factor for numerical accuracy and efficiency. In some cases, higher order Taylor series approximations, or Newton's iteration method have to be used to insure convergence of the numerical solutions.

Finally, the equation for the pressure terminal is trivial. Based on the previous discussion, it is

$$i_P(t) = \begin{pmatrix} 0 & 0 & 0 & 1 \end{pmatrix} \begin{pmatrix} v_0(t) \\ v_1(t) \\ T(t) \\ P(t) \end{pmatrix} - (b_P(t-h)) \tag{17}$$

and

$$b_P(t-h) = -i_P(t-h) + P(t-h) \quad (18)$$

4. Example applications

We present here three system applications that illustrate some of the capabilities of VTB.

4.1. Electric vehicle

Fig. 2 shows an electric vehicle system that illustrates several VTB features. The system contains several electrochemical power sources, including fuel cell, battery, and supercapacitor. These components are coupled to a model of the mechanical subsystem which was imported as ACSL-generated executable code.

The model also includes power distribution and control subsystem (converters, controllers and sensors), and a driver command subsystem (acceleration/deceleration command and steering wheel) for interactive simulations. Even still, the system is greatly simplified. The system is currently used to study the interactions between the power system components under various operating conditions.

In the case study shown by the dashed curve in Fig. 3, the driver commands the vehicle to accelerate for 20 s until cruising speed (28 m/s, or 60 mile/h) is reached, then maintains that speed for 20 s, and then decelerates (beginning at 40 s) until the vehicle stops. Total time shown in the figure is 65 s. The solid curve shows the vehicle speed.

Power profiles are shown in Fig. 4 for the load, the supercapacitor, the battery and the fuel cell The time scale is expressed in percentage of 65 s. During the 20 s acceleration period, the load drew a power that peaked at 86.7 kW

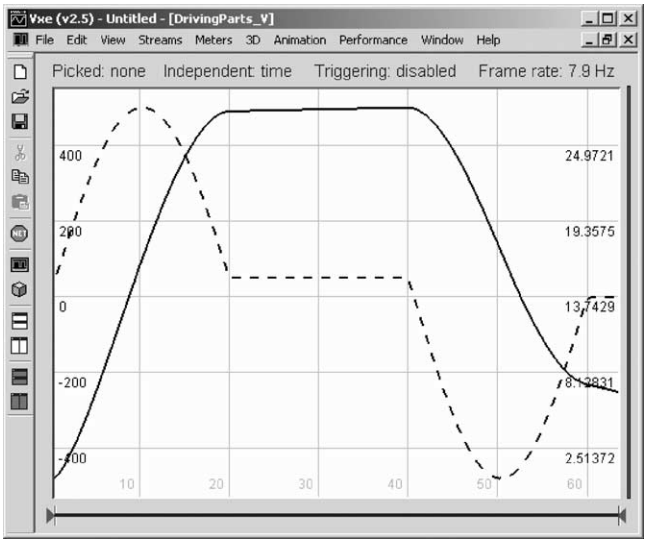

Fig. 3. Driver commanded torque (dashed and left scale) and the vehicle speed (solid and right scale).

(116 hp). During the first 10 s of acceleration, a majority of the power was provided by the supercapacitor bank. Stress on the fuel cell and the battery were significantly decreased by the presence of the capacitor. Analysis shows [11] that operating the battery or fuel cell in conjunction with the supercapacitor not only prevents over-current of the battery and the fuel cell, but also extends discharge lifetime of a battery, owing to a reduction of internal power dissipation. At about 15 s, the capacitor started to recharge while the fuel cell and the battery assumed the full load power demand. From 20 to 40 s, the capacitor continued to store excess power delivered by the fuel cell. The load power became negative after 40 s during the braking period, and energy flowed back to the capacitor bank, and some to the battery.

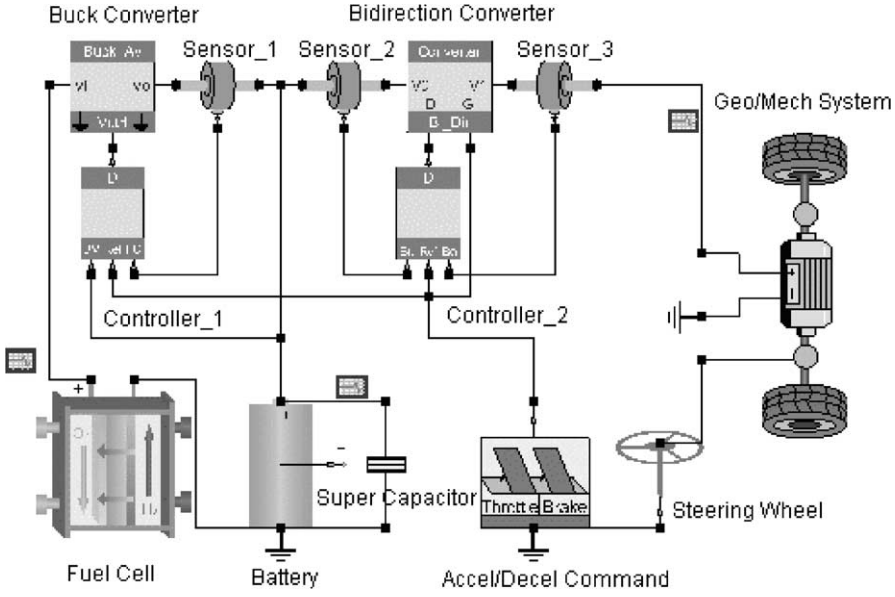

Fig. 2. An electric vehicle fuel cell, lithium-ion battery and supercapacitor as power sources.

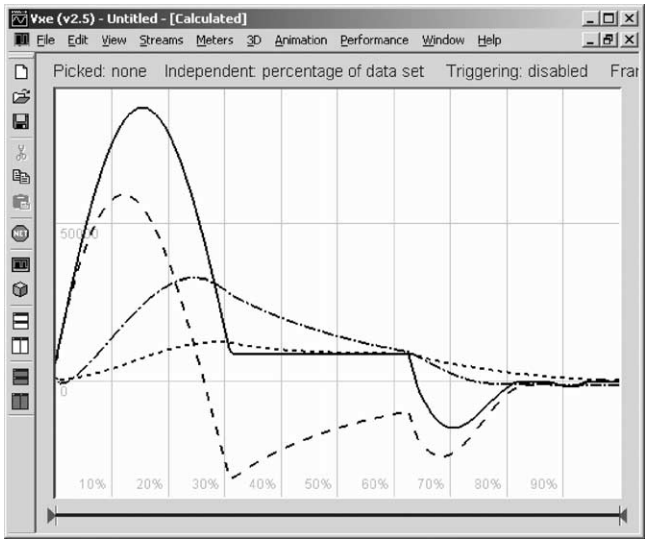

Fig. 4. Power profiles for the load (solid), supercapacitor (dashed), battery (dotted) and fuel cell (dot-dashed). The supercapacitor carries most of the instantaneous load.

Fig. 5 shows a screen shot of the three-dimensional visualization in action. The trace of the vehicle path that is visible in the figure is a result of an arbitrary driving command provided by the user. The user can directly see the dashboard instruments, or graph any other variables output by the simulation.

4.2. Small portable power systems

The goal of this work is to design a power converter topology and control system that will allow a polymer electrolyte membrane fuel cell and a lithium-ion battery pack to safely interact while sharing the power demands of the load. This example is included here because it illustrates the capability for interactive coupling to Matlab/Simulink. To accomplish our goal, we must insure that the average current output of the particular PEM fuel cell will not exceed 3 A for ''long'' durations (because of water management issues), that the battery pack never charges at greater than 1.4 A, and that the battery pack voltage never exceeds 16.4 V.

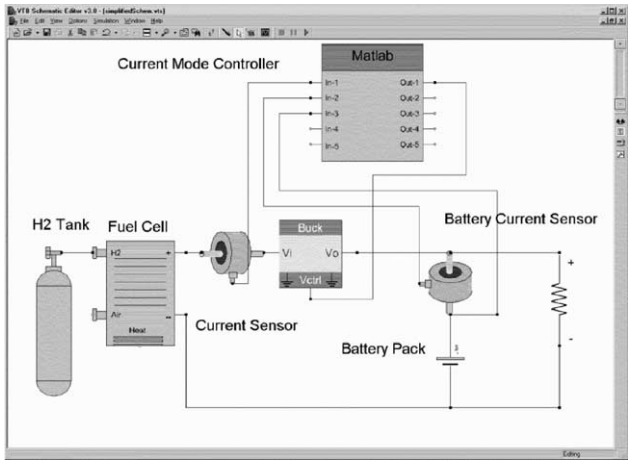

Fig. 6. Simplified schematic of the fuel cell—battery hybrid power source.

Fig. 6 shows a simplified schematic of the system. The basic components are the PEM fuel cell, current mode buck converter, lithium-ion battery pack, load, and controller. The controller was based on a commercially available current

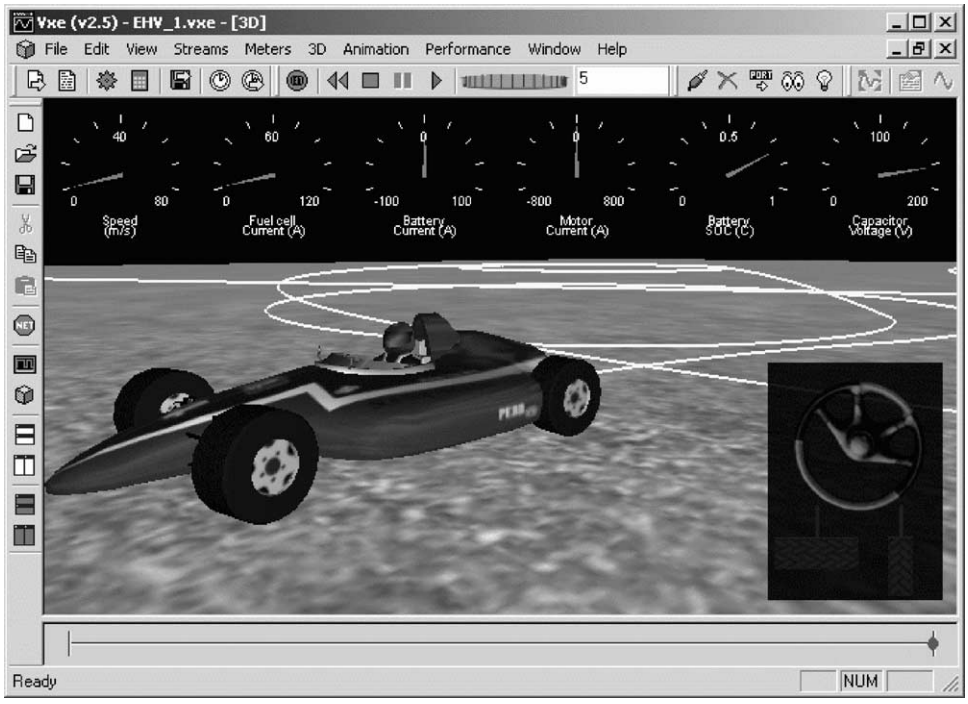

Fig. 5. Three-dimensional visualization of the performance of an electric vehicle, including dashboard instruments, and steering wheel for user interaction.

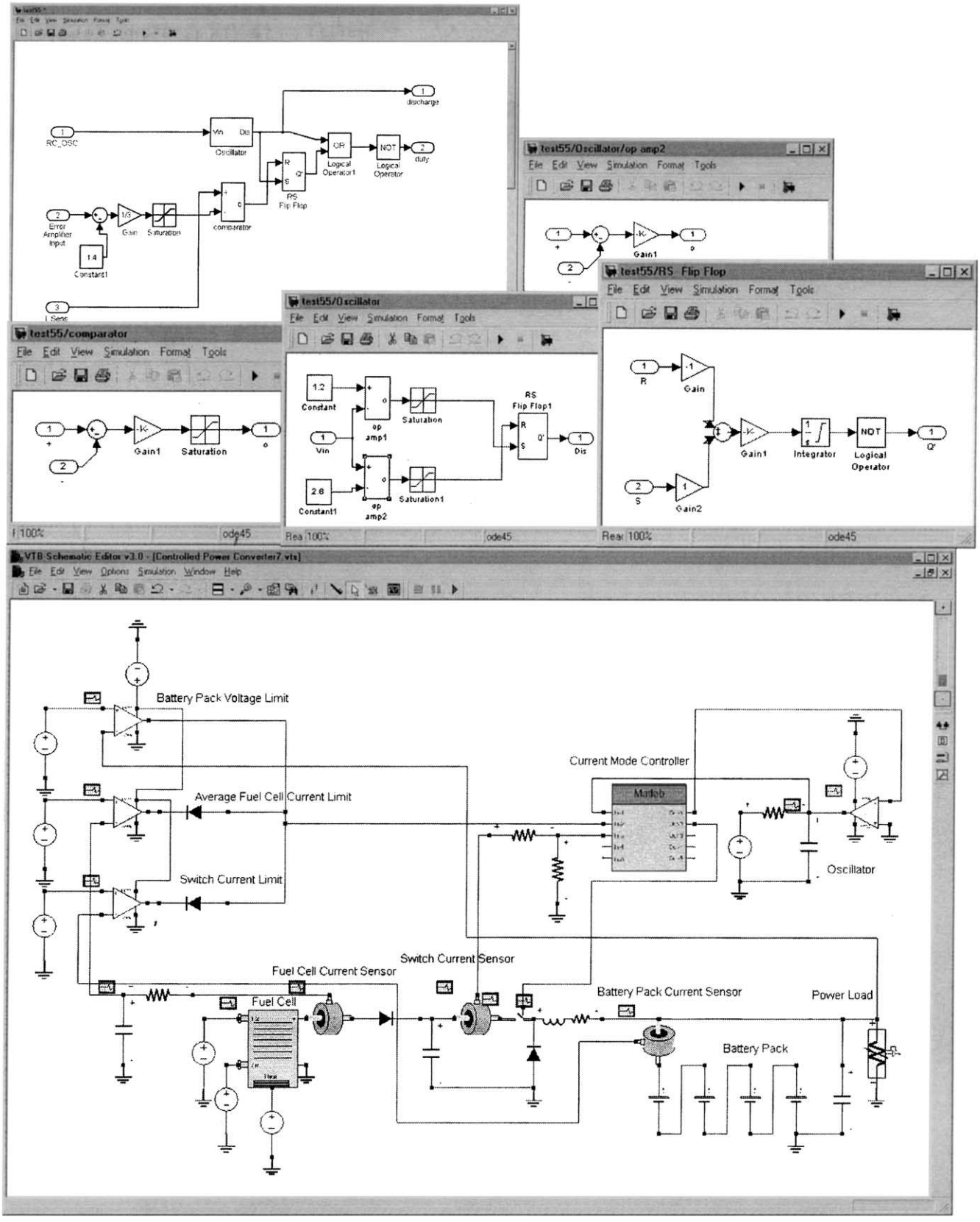

Fig. 7. More complete schematic, showing details of the control implementation.

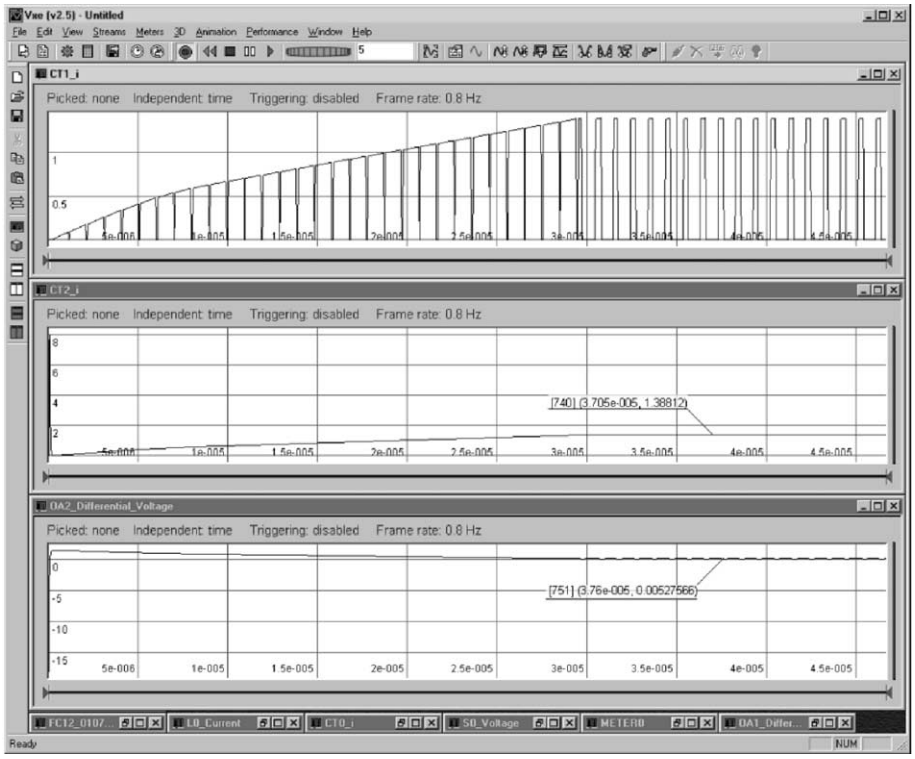

Fig. 8. Top—transistor current in the buck converter. Middle—battery current. Bottom—difference between actual and set battery current. This shows proper limitation of battery charging current.

mode controller with added control states and feedback. The control algorithm was prototyped using a mixture of VTB native models and MATLAB/Simulink models. Fig. 7 shows the full complexity of the system, and details of the controller implementation using standard Simulink blocks.

Fig. 8 shows the results of a test which studied charging of a depleted battery. This test evaluated the feedback control loops that set maximum charge current and the maximum average fuel cell current. At the beginning of the simulation, the output filter inductor must charge to operating energy.

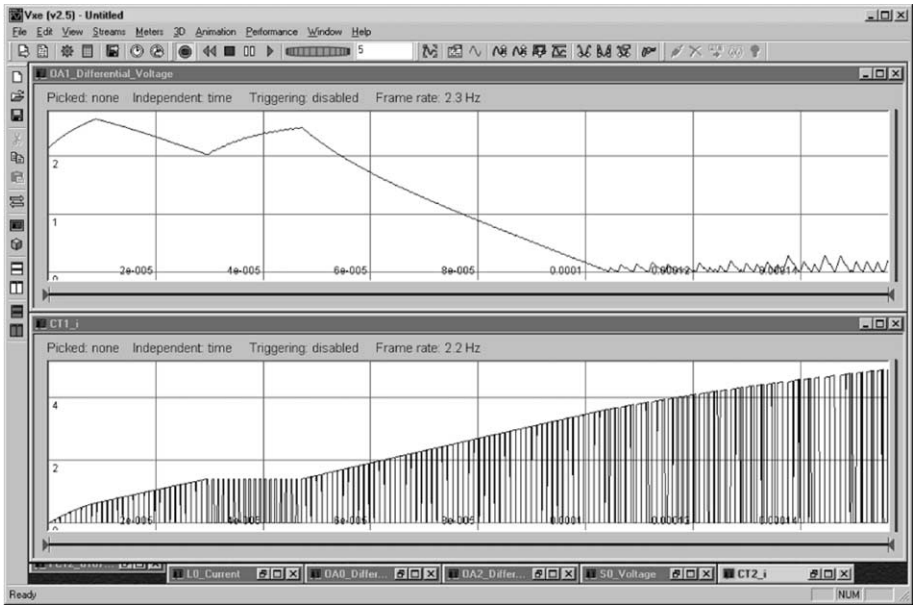

Fig. 9. Top—difference between safe limit value of fuel cell current and actual average current. Bottom—transistor current in the buck converter. This demonstrates correct limitation of average fuel cell current. Oscillations of pulse width are due to lack of slope compensation in the controller.

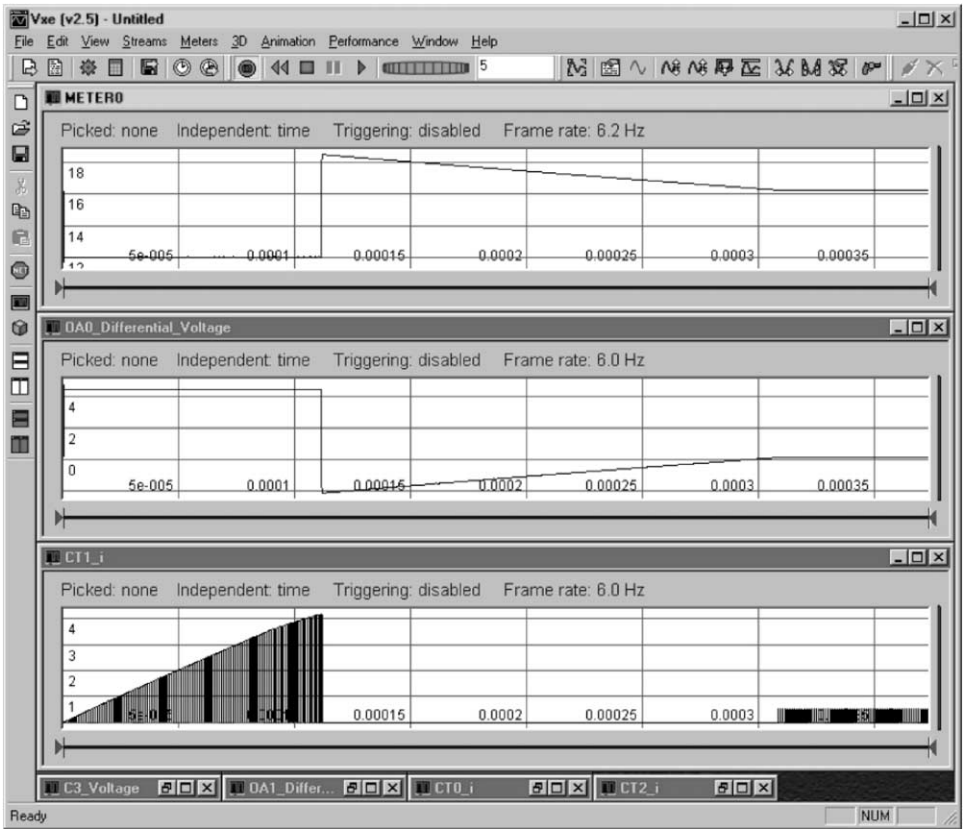

Fig. 10. Top—battery voltage. Middle—difference between battery voltage limit and actual battery voltage. Bottom—transistor current. This shows proper limiting of the battery voltage at full charge condition, and response to a load dump.

At this point, the maximum battery pack current is limited on a cycle-by-cycle basis. The topmost data trace is the instantaneous transistor current, middle is the battery charging current, and lowest is the error of the charging current with respect to the desired value.

Fig. 9 illustrates how the controller enforces a limit on the average PEM fuel cell current. After the filter inductor ramps up to operating energy, there are duty ratio oscillations in the control path. This is due to the fact that slope compensation is needed for duty ratios higher than 50%. At this time, slope compensation has not been implemented in the control topology to address the problem of pulse width oscillation. The topmost trace is the state error with respect to the desired value and the lowest trace is the instantaneous transistor current. The duty ratio oscillations are clearly visible in the state error graph.

Fig. 10 shows the response to reaching the battery voltage limits. The topmost waveform is the battery pack voltage, middle is the state error with respect to the desired value, and the bottom is the instantaneous transistor current. At first, the system reaches operating conditions while under a heavy load. The duty ratio oscillations are evident in this operating condition. Then the load is reduced to a relatively light load. At this point, the battery pack was already nearly fully charged, so that the majority of the power supplied by the fuel cell was being delivered to the external load. Under the rapid load shedding, the excess energy stored in the filter inductor briefly (200 μs) forced the voltage above the maximum safe operating voltage of the battery pack. That should not present any serious problems, however, because the low energy content of the power spike was small (mJ).

4.3. Satellite power systems

Fig. 11 shows a good demonstration of a multidisciplinary system, including heat transfer, in the form of a satellite electric power system. The objective of the study is to understand the cycling characteristics of the nickel hydrogen battery during the satellite's orbit. A solar array converts sunlight into electric power which is then stored in the nickel hydrogen battery. The battery provides power to the load during maneuvers that take the solar arrays out of the sunlight or during eclipse periods. Battery charging is controlled by a controlled buck converter. Power auctioneering diodes ensure that power is drawn from the most appropriate source at any time. Notice that the solar array is connected to a radiator for heat dissipation, while the battery is connected to the ambient through a conduction cooling mechanism model.

Fig. 12 shows simulation results for the behaviors of the battery and its interaction with the solar array under a variety of conditions. The solar array output voltage and current show that the satellite has an orbit period of 94 min with

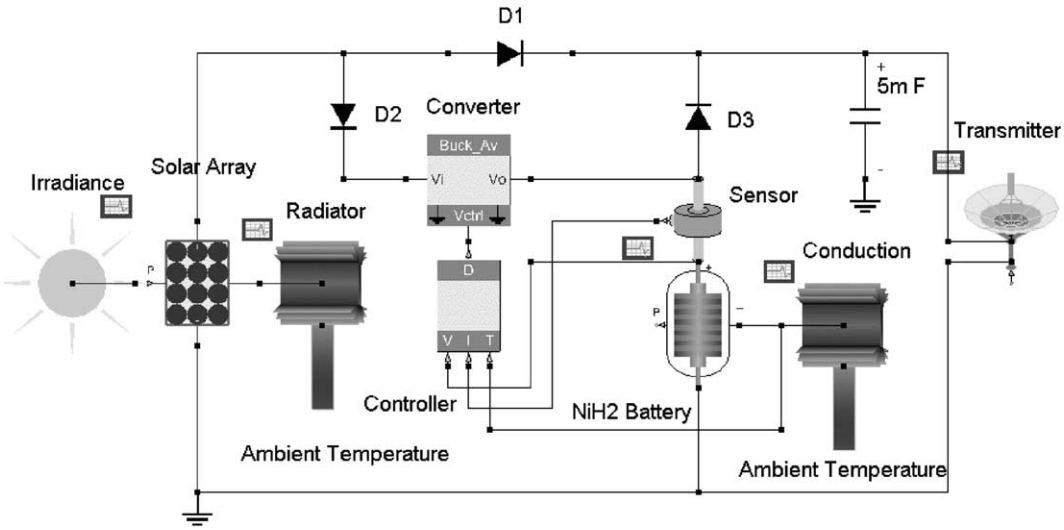

Fig. 11. An example satellite electric power system using nickel hydrogen battery.

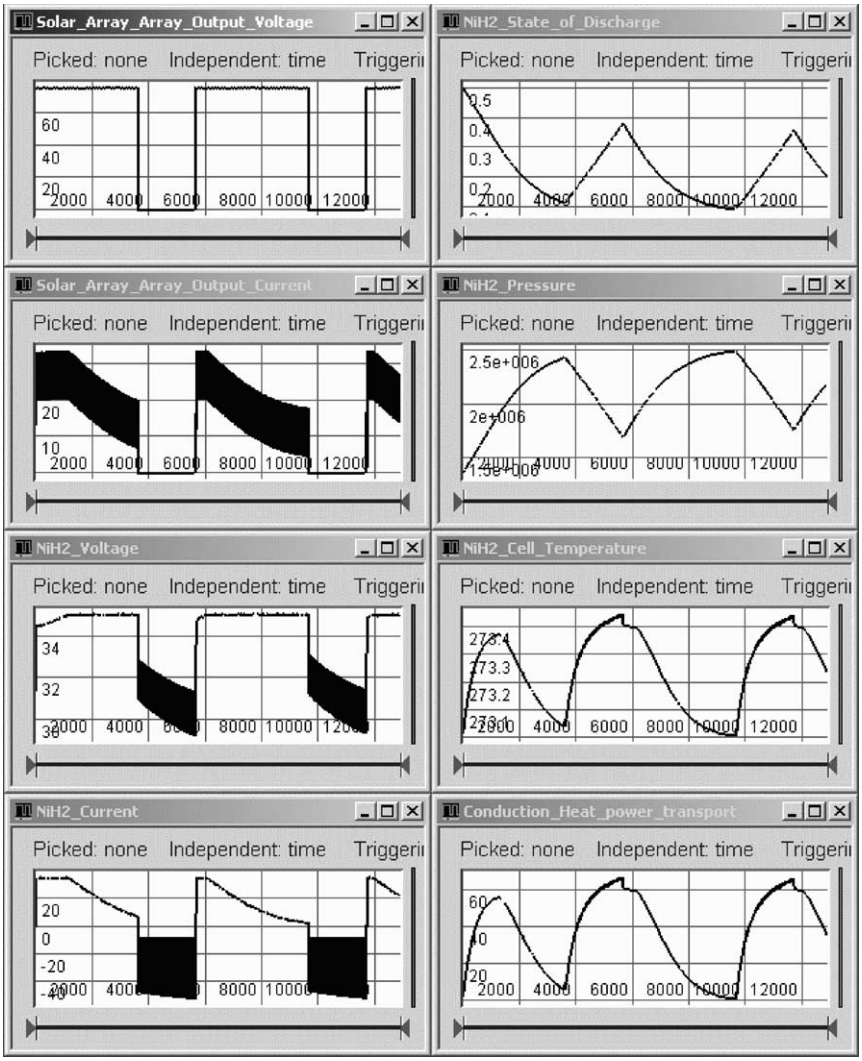

Fig. 12. Dynamic simulation results of the satellite power system.

eclipse about 33.6 min. The solar array provides power to both the load and the battery during illumination, and shuts down during eclipse. The solar array voltage is about 75 V, while the current has considerable ripples due to the pulsed power demand of the transmitter.

For the first 19.5 min, the battery is charged at a constant current (35 A), as set by the controller. Associated with the charging process is the nickel reduction that yields hydrogen pressure (Pa) increase, state-of-discharge decrease, and the battery voltage increase.

The maximum battery voltage is set at 35 V by the controller to protect the battery from overcharge. The battery charging mode changes from constant current to constant voltage when the voltage reaches 35 V, and the current immediately tapers down. During this time, the hydrogen pressure continues to increase, though at a slower rate.

During eclipse, the battery provides power to the load, which is indicated by the negative current. Correspondingly, the hydrogen pressure decreases and the state-of-discharge increases. The voltage ripples are caused to the pulsed power load.

The ambient temperature and the initial temperature of the battery are both set to 273 K (the valid temperature range for the battery model is from 200 to 400 K). In practice, the nickel hydrogen battery in spacecraft is mounted in a heat source so that a constant temperature can be obtained. Here, a constant temperature for the ambient and initial temperature is used to simulate that situation. From the temperature curve in Fig. 12, we see that the battery temperature is above the ambient during the operation, but with a maximum excursion of only 0.5 K during the first two orbits. It always increases during discharge, because both resistive heating and entropy change release heat. The temperature also increases during the high-current (35 A) charging phase, but it decreases during periods of low-current charging because then the heat uptake due to entropy change is larger than the ohmic losses.

5. Conclusions

We have described how the VTB can be used to study the performance of power sources in the system context. The ready availability of the VTB software, of accurate models of advanced electrochemical power sources, and models of equipment that can be powered by those sources make this environment useful to study the design and performance of advanced power sources. The further capabilities to interactively link to other software such as Matlab/Simulink, and to interact through the visualization environment add to this value. The open environment encourages contribution of models by others.

Acknowledgements

The work described here is supported by a variety of sources including the US Office of Naval Research (grant N00014-00-1-0131), and the NRO (grant NRO-00-C-0134). The contributions to formulation of the electrochemical component models by Professors. J. Weidner, R.E. White, and others in USC Chemical Engineering Department are gratefully acknowledged.

References

[1] R.A. Dougal, C.W. Brice, R.O. Pettus, G. Cokkinides, A.P.S. Meliopoulos, Virtual-prototyping of PCIM systems—the virtual test bed, in: Proceedings of the PCJM/HFPC'98 Conference, Santa Clara, CA, November 1998, pp. 226–234.
[2] M.R. Lightner, S.W. Director, Computer-aided design of electronic circuits, in: D.G. Fink, D. Christiansen (Eds.), Electronics Engineers' Handbook, 3rd Edition, Section 27, McGraw-Hill, New York, 1989.
[3] VHDL Analog and Mixed-Signal Extensions, IEEE Standards 1076.1-1999, March 1999.
[4] S. Liu, R.A. Dougal, Dynamic multi-physics model for solar array, submitted for publication.
[5] B. Wu, R.E. White, Self-discharge model of a nickel hydrogen cell, J. Electrochem. Soc. 147 (3) (2000) 902–909.
[6] B. Wu, R.E. White, Modeling of a nickel hydrogen cell, phase reaction in the nickel active material, J. Electrochem. Soc. 148 (6) (2001) A595–609.
[7] K.P. Ta, J. Newman, Proton intercalation hysteresis in charging and discharging nickel hydroxide electrodes, J. Electrochem. Soc. 146 (8) (1999) 2769–2779.
[8] V. Srinivasan, J.W. Weidner, J. Newman, Hysteresis during cycling of nickel hydroxide active material, J. Electrochem. Soc. 148 (9) (2001) A969–980.
[9] M. Jam, A.L. Elmore, M.A. Mathews, J.W. Weidner, Thermodynamic consideration of the reversible potential for the nickel electrode, Electrochem. Acta 43 (18) (1998) 2649–2660.
[10] D. Bernardi, E. Pawlikowski, J. Newman, A general energy balance for battery systems, J. Electrochem. Soc. 132 (1) (1985) 5–12.
[11] R.A. Dougal, S. Liu, R. White, Power and life extension of battery/ultracapacitor hybrids, IEEE Trans. Components Packaging Technol., submitted for publication.